PROCEEDINGS OF SCIENCE

The pion scalar form factor with $N_f = 2 + 1$ Wilson fermions

Konstantin Ottnad[a,*] **and Georg von Hippel**[a]

[a] *PRISMA$^+$ Cluster of Excellence and Institut für Kernphysik, Johannes Gutenberg-Universität Mainz, Johann-Joachim-Becher-Weg 45, 55099 Mainz, Germany*

E-mail: kottnad@uni-mainz.de

We report preliminary results from an analysis of the pion scalar form factor computed on a set of the $\mathrm{tr}[M]$ = const CLS gauge ensembles with $N_f = 2 + 1$ Wilson Clover-improved sea quarks. The calculations are carried out for light quarks masses corresponding to $M_\pi \approx 0.130\text{MeV} \ldots 350\text{MeV}$, four values of the lattice spacing $a \approx 0.049\,\text{fm} \ldots 0.086\,\text{fm}$ and a large range of physical volumes. A fine-grained momentum resolution is achieved by allowing for non-vanishing sink momenta and by including two particularly large and fine boxes close to physical quark masses (i.e. $T \times L^3 = 192 \times 96^3$, $M_\pi \leq 172\text{MeV}$, $a \leq 0.064\,\text{fm}$). The pertinent quark-disconnected contributions have been computed to high precision using a scheme combining 1.) the one-end trick on stochastic volume sources for the computation of differences between two quark flavors with 2.) the hopping parameter expansion and hierarchical probing to evaluate the loops for the heaviest, single quark flavor.

The 40th International Symposium on Lattice Field Theory (Lattice 2023)
July 31st - August 4th, 2023
Fermi National Accelerator Laboratory

*Speaker

PoS(LATTICE2023)313

1. Introduction

The scalar form factor of the pion

$$F_S^{\pi,l}(Q^2) = \langle \pi(p_f)|m_d\bar{d}d + m_u\bar{u}u|\pi(p_i))\rangle\,, \tag{1}$$

is not directly accessible to experiment. Still, the corresponding radius

$$\langle r_S^2\rangle_\pi^l = \frac{-6}{F_S^{\pi,l}(0)}\left.\frac{dF_S^{\pi,l}(Q^2)}{dQ^2}\right|_{Q^2=0}, \tag{2}$$

is relevant to the low-energy regime of QCD as it is related to the $\pi\pi$ scattering cross section [1–3]. Furthermore, it enters the chiral expansion of the pion decay constant in two-flavor chiral perturbation theory [4]

$$1\frac{F_\pi}{\mathring{F}_\pi} = 1 + \frac{1}{6}M_\pi^2\langle r_S^2\rangle_\pi^l + \frac{13M_\pi^2}{192\pi^2F_\pi^2} + \mathcal{O}(M_\pi^4)\,. \tag{3}$$

The next-to-leading order expression for $\langle r_S^2\rangle_\pi^l$ depends only on a single low-energy constant $\bar{l}_4$,

$$\langle r_S^2\rangle_\pi^l = \frac{1}{(4\pi f)^2}\left[-\frac{13}{6} + \left(6\bar{l}_4 + \log\left(\frac{M_{\pi,\text{phys}}^2}{M_\pi^2}\right)\right)\right]. \tag{4}$$

In principle, this allows to obtain a rather straightforward, model-independent determination of $\bar{l}_4$ from lattice QCD. Nevertheless, only few modern lattice calculations exist in literature [5–7], arguably none of them with fully controlled systematics. A complication arises from the notorious quark-disconnected contributions to the pion scalar form factor which render such a calculation computationally and conceptually more demanding than e.g. a study of vector form factors.

Beyond the two-flavor theory contributions of the strange quark to the pion scalar form factor are conveniently parameterized in terms of SU $(3)_F$ octet and singlet combinations. Lattice results for the corresponding radii $\langle r_S^2\rangle_\pi^8$ and $\langle r_S^2\rangle_\pi^0$ are even more scarce [7] than for $\langle r_S^2\rangle_\pi^l$ as effects of the strange quark are mediated entirely by quark-disconnected diagrams. Still, due to the relatively large quark-disconnected contributions particularly at zero and small momentum transfer, the effects of the strange quark are not negligible, leading to an expected hierarchy of the radii, i.e. $\langle r_S^2\rangle_\pi^8 < \langle r_S^2\rangle_\pi^l < \langle r_S^2\rangle_\pi^0$ assuming $m_l < m_s$.

2. Lattice setup

Our lattice calculations are carried out on gauge ensembles with $N_f = 2 + 1$ flavors of non-perturbatively $\mathcal{O}(a)$-improved Wilson fermions [8] and the tree-level Symanzik-improved Lüscher-Weisz gauge action [9]. These ensembles have been generated by the Coordinated Lattice Simulation (CLS) consortium [10] employing a twisted mass regulator in the (mass-degenerate) light quark sector to suppress exceptional configurations [11] and the rational approximation [12] for the dynamic strange quark. For the required reweighting of physical observables we employ reweighting factors computed using exact low mode deflation, cf. Ref. [13]. The only exception is the E300

Table 1: List of CLS gauge ensembles used in this work. Open and periodic boundary conditions in time are indicated by superscripts "o" and "p", respectively. N_{conf} is the number of gauge configurations on which the $N^{\text{3pt}}_{\text{meas}}$ ($N^{\text{2pt}}_{\text{meas}}$) measurements of three-point (two-point) functions have been performed. ΔN_{conf} denotes the index stride between gauge configurations with measurements and the last column lists the available values of t_{sep}/a.

ID^{BC}	a/fm	T/a	L/a	M_π/ MeV	N_{conf}	ΔN_{conf}	$N^{\text{3pt}}_{\text{meas}}$	$N^{\text{2pt}}_{\text{meas}}$	t_{sep}/a
C101^o	0.086	96	48	222	1973	1	15784	276220	11, 15, 19, 23, 27, 31, 35
N101^o		128	48	279	1260	1	10080	176400	
H105^o		96	32	285	1011	1	8088	141540	
H102^o		96	32	351	1020	1	8160	142800	
D450^p	0.076	128	64	218	497	1	3976	63616	13, 17, 21, 25, 29, 33, 37, 41
N451^p		128	48	287	1003	1	8024	128384	
S400^o		128	32	357	994	2	7952	127232	
E250^p	0.064	192	96	132	491	2	3928	62848	15, 21, 27, 33, 39, 45, 51
D200^o		128	64	202	991	2	7928	138740	
N200^o		128	48	285	1705	1	13640	238700	
N203^o		128	48	346	1535	1	12280	214900	
E300^o	0.049	192	96	174	569	2	4552	79660	19, 27, 35, 43, 51, 59, 67
J303^o		192	64	256	1068	1	8544	149520	

ensemble, for which stochastic estimators have been used as discussed in Ref. [10]. An overview of the 13 ensembles currently used in this study can be found in Table 1. For further details we refer to Ref. [10]. Moreover, we remark that we make use of the procedure developed in Ref. [14] to deal with positivity violations of the fermion determinant that affect a small subset of gauge configurations on some ensembles. At present we have only included ensembles that lie on the chiral trajectory defined by the constraint $\text{tr}[M] = 2m_l + m_s = \text{const}$ for the quark mass matrix M.

Whenever conversion to physical units is required, we use the values for t_0^{sym}/a^2 from Ref. [15] determined at the symmetric point together with the world average for the gradient flow scale t_0 [16] given by FLAG in Ref. [17], i.e. $t_0^{\text{phys}} = 0.14464(87)$. At this stage of the analysis we do not yet carry out the physical extrapolation of our lattice results, hence the scale only enters in the values of M_π in Table 1 and in results for scalar radii in physical units on individual ensembles. Besides, the values for the lattice spacings quoted in Table 1 corresponding to the four values of $\beta \in \{3.40, 3.46, 3.55, 3.70\}$ have been computed from this procedure as well.

2.1 Computational details

A lattice study of the pion scalar form factor requires the evaluation of quark-connected and disconnected three-point functions depicted in Fig. 1. The basic building blocks are quark-disconnected loops

$$C^{\text{1pt}}(\mathbf{p}, t) = \sum_{\mathbf{x}} e^{i\mathbf{p}\cdot\mathbf{x}} \langle \mathcal{S}_f(\mathbf{x}, t) \rangle_F \,,$$

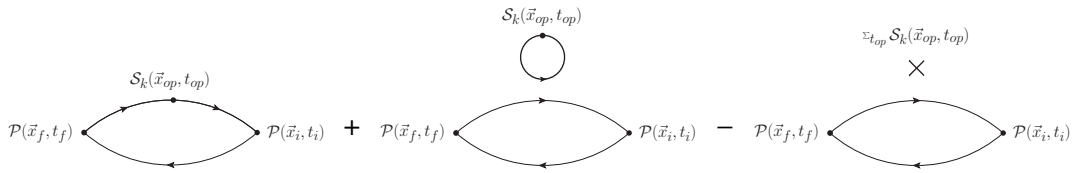

Figure 1: Quark-connected and disconnected contributions to the three-point function in Eq. (6). The last diagram contributes only for vanishing loop momentum.

and quark-connected two- and three-point functions

$$C^{\text{2pt}}(\mathbf{p}, \mathbf{x}_i, t_f - t_i) = \sum_{\mathbf{x}_f} e^{i\mathbf{p}\cdot(\mathbf{x}_f - \mathbf{x}_i)} \langle \mathcal{P}(\mathbf{x}_f - \mathbf{x}_i, t_f - t_i) \mathcal{P}^\dagger(\mathbf{0}, 0) \rangle \,, \tag{5}$$

$$C_k^{\text{3pt}}(\mathbf{p}_f, \mathbf{q}, \mathbf{x}_i, t_{\text{sep}}, t_{\text{ins}}) = \sum_{\mathbf{x}_f, \mathbf{x}_{op}} e^{i\mathbf{p}_f\cdot(\mathbf{x}_f - \mathbf{x}_i)} e^{i\mathbf{q}\cdot(\mathbf{x}_{op} - \mathbf{x}_i)} \langle \mathcal{P}(\mathbf{x}_f - \mathbf{x}_i, t_{\text{sep}}) \mathcal{S}_k(\mathbf{x}_{op} - \mathbf{x}_i, t_{\text{ins}}) \mathcal{P}^\dagger(\mathbf{0}, 0) \rangle \,, \tag{6}$$

where $\mathcal{P}(x) = u(x)\gamma_5 \bar{d}(x)$ denotes the interpolating operator for the pion and $t_{\text{sep}} = t_f - t_i$, $t_{\text{ins}} = t_{op} - t_i$ are shorthands for the pertinent Euclidean time-separations. In addition to a scalar operator insertion involving only light quarks, $\mathcal{S}_l = \bar{u}u + \bar{d}d$, we also compute the octet and singlet flavor combinations involving the strange quark, i.e. $\mathcal{S}_8 = \bar{u}u + \bar{d}d - 2\bar{s}s$ and $\mathcal{S}_0 = \bar{u}u + \bar{d}d + \bar{s}s$.

For the computation of the quark-disconnected loops we employ stochastic volume sources and the one-end trick [18] to obtain a frequency splitting estimator [19] in combination with the generalized hopping parameter expansion [5] and hierarchical probing [20]. For further details on the setup we refer to Ref. [21].

The quark-connected two- and three-point functions are evaluated on and averaged over point sources. The actual source setup depends on the boundary conditions used in time on a given ensemble, cf. Table 1. For ensembles with periodic boundary conditions (pBC) sources are drawn randomly without replacement with the only constraint arising from the combination of the truncated solver method with the Schwartz alternating procedure (SAP) preconditioning [22, 23]. The three-point functions are computed using the sequential sink method with the final state either produced at rest or with one unit of momentum $\mathbf{p}_f = (1,0,0)^T$. For ensembles with pBC we use eight sources per gauge configuration for the three-point functions, which is reflected by the numbers for $N_{\text{meas}}^{\text{3pt}}$ in Table 1. The forward propagators are re-used for all values of t_{sep} as well as for the computation of two-point functions. Additional 120 sources per gauge configuration are used to increase the two-point function statistics for the computation of quark-disconnected (2+1)-point functions, resulting in much larger numbers for $N_{\text{meas}}^{\text{2pt}}$. For ensembles with open boundary conditions (oBC) four sources are randomly placed on each of the two possible source timeslices symmetric around $T/2$ for each value of t_{sep} for the computation of three-point functions. Additional two-point functions are computed on the same set of timeslices to achieve a similar $N_{\text{meas}}^{\text{2pt}}/N_{\text{conf}}$ ratio as for ensembles with pBC.

However, a subtlety arises for the computation of quark-disconnected (2+1)-point functions on ensembles with oBC. While for pBC two-point functions computed on any point source can be used in forward and backward time direction, such averaging is limited on ensembles with oBC as a safe distance from the boundaries needs to be kept for the operator insertion in t_{op} to avoid

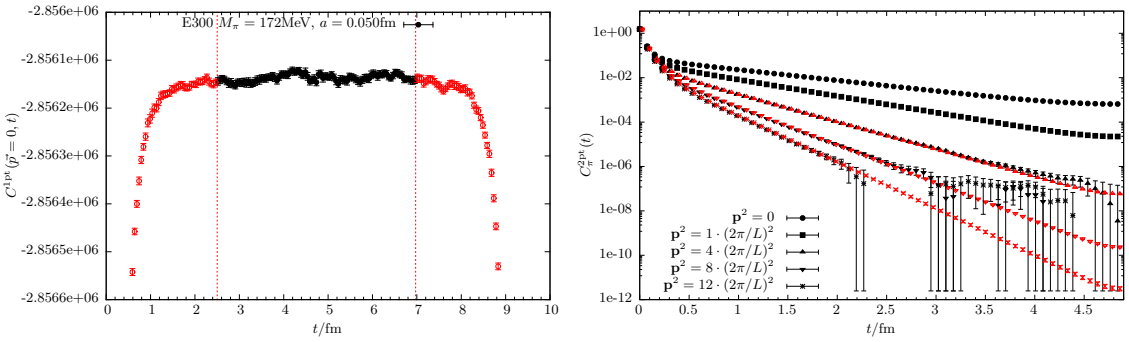

Figure 2: Left panel: Scalar one-point function on the E300 ensemble with open boundary conditions in time. Red data are excluded in the construction of quark-disconnected (2+1)-point functions. Right panel: Pseudoscalar two-point functions for several momenta on the D450 ensemble. For $\mathbf{p}^2 \geq 4 \cdot (2\pi/L)^2$ the large-t tail has been reconstructed (red points) from a fit to data at smaller values of t. Corresponding data points are horizontally displaced for legibility.

contamination by boundary effects. The range that needs to be excluded can be readily assessed from the time-dependence of the scalar loop at zero-momentum transfer and can be as large as $t_{\mathrm{ex}} = 2.5$ fm depending on M_π as shown in the left panel of Fig. 2 for the most chiral ensemble with oBC. In particular, at larger values of t_{sep} and for ensembles with smaller physical time extent this can lead to greatly reduced effective statistics for these measurement compared to ensembles with pBC.

Statistical errors are computed using the binned jackknife method, and we adopt the procedure previously used in Refs. [24–26] for the computation of isoscalar observables in the nucleon sector to identify individual measurements on a few point sources that represent extreme outliers and would cause unduly inflated statistical errors. The affected gauge configurations have been excluded from further analysis which is taken into account in the numbers for N_{conf} in Table 1.

3. Form factor extraction

In a first step to extract the scalar matrix element we compute effective form factors from the standard ratio of two- and three-point functions

$$R(p_f^2, q^2, p_i^2, t_f - t_i, t_{op} - t_i) = \frac{C_3(p_f^2, q^2, p_i^2, t_f - t_i, t_{op} - t_i)}{C_2(p_f^2, t_f - t_i)} \cdot \sqrt{\frac{C_2(p_i^2, t_f - t_{op}) C_2(p_f^2, t_{op} - t_i) C_2(p_f^2, t_f - t_i)}{C_2(p_f^2, t_f - t_{op}) C_2(p_i^2, t_{op} - t_i) C_2(p_i^2, t_f - t_i)}}. \tag{7}$$

which yields the desired ground state matrix elements $\langle \pi(p_f^2) | \mathcal{S}_k(q^2) | \pi(p_i^2) \rangle \sim F_S^{\pi,k}(Q^2)$ at asymptotically large Euclidean time separations. While the two- and three-point functions for the pion generally exhibit a constant signal-to-noise ratio at zero-momentum, they develop a signal-to-noise problem at increasing momentum transfer, as shown in the right panel of Fig. 2 for the the case of the two-point functions on D450 . In order to alleviate this issue in the construction of the ratio in Eq. (7) for larger values of t_{sep} we fit the ground-state contribution to the two-point

functions at $p^2 \geq 2 \cdot (2\pi/L)^2$ and replace the corresponding two-point function data by the fit result, which is illustrated by the red data points in the right panel of Fig. 2. Example data for the light, quark-connected contribution as well as the quark-disconnected light, octet and singlet contributions to the effective form factors at vanishing transfer and $\mathbf{p}_f = (0,0,0)^T$ are shown in Fig. 3. The quark-disconnected contributions for $F_S^{\pi,l}$ and $F_S^{\pi,0}$ can reach similar size as the quark-connected piece at $q^2 = 0$ depending on the lattice spacing and light quark mass, in agreement with expectations from chiral perturbation theory [27]. However, their relative (and absolute) size decreases at increasing momentum transfer.

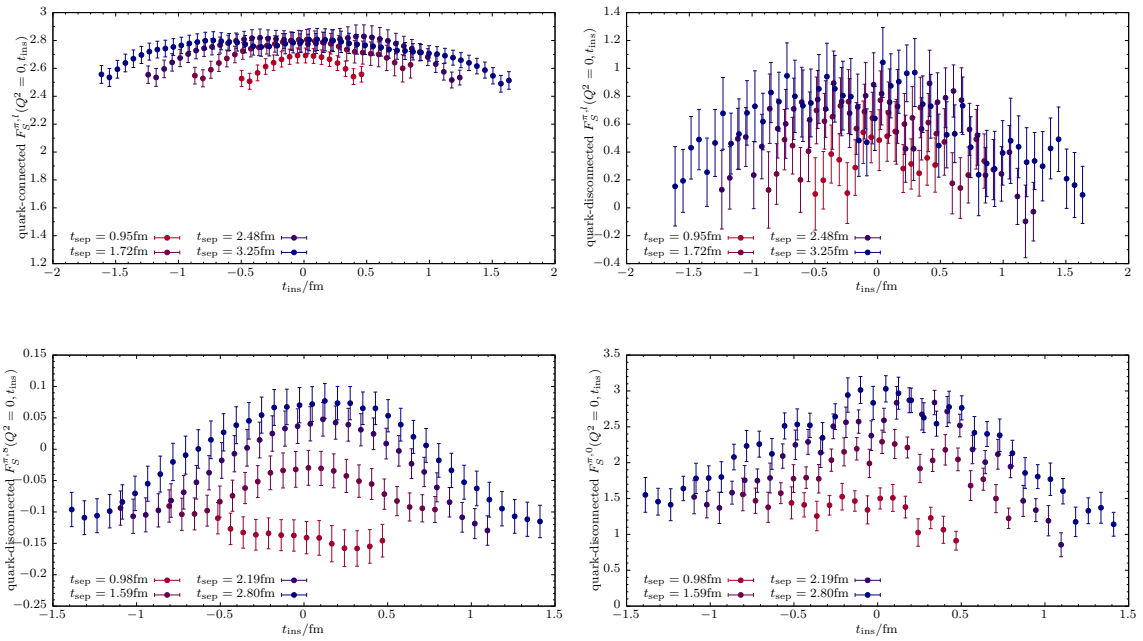

Figure 3: Effective form factors at $Q^2 = 0$ with $\mathbf{p}_f = (0,0,0)^T$. Upper row: Light quark-connected (left panel) and quark-disconnected contribution on the E250 ensemble. Lower row: Octet (left panel) and singlet (right panel) quark-disconnected contribution on the N451 ensemble. Data for every second available value of $t_{\rm sep}$ are included.

In order to gain further suppression of excited states we employ the summation method [28–30]

$$S(p_f^2, q^2, p_i^2, t_{\rm sep}) = \sum_{t_{\rm ins}=t_0}^{t_{\rm sep}-t_0} R(p_f^2, q^2, p_i^2, t_{\rm sep}, t_{\rm ins}) \\ = \text{const} + \langle \pi(p_f^2)|S(q^2)|\pi(p_i^2)\rangle (t_{\rm sep} - t_0) + \mathcal{O}(e^{-\Delta t_{\rm sep}}) \,, \tag{8}$$

where Δ is the mass gap between ground and first excited state and we choose $t_0 = 0.4\,\text{fm}$. We find this choice to improve the signal quality for non-vanishing source and sink momenta, while still leaving enough points in the sum at smaller values of $t_{\rm sep}$. For the preliminary analysis in this proceedings contribution we include data for $t_{\rm sep} \gtrsim 1.0\,\text{fm}$ up to $t_{\rm sep} \lesssim 3.5\,\text{fm}$. However, the application of the summation method turns out to be challenging on a few ensembles with oBC due to the aforementioned, drastic reduction in effective statistics at $t_{\rm sep} \gtrsim 2\,\text{fm}$ in the disconnected

contribution depending on the excluded time range t_{ex} next to the boundary and the value of T. On the affected ensembles we observe a systematic deviation at small Q^2 for $t_{\text{sep}} \gtrsim 2\,\text{fm}$ from the expected linear behavior in Eq. (8) towards larger slopes, which leads to an overestimation of $F_S^{\pi,k}(Q^2)$. Since the quark-connected contribution is not subjected to such a reduction in statistics as function of t_{sep}, the effect is most prominent in $F_S^{\pi,l}(Q^2)$ and $F_S^{\pi,0}(Q^2)$, whereas the octet combination $F_S^{\pi,8}(Q^2)$ is less affected. In the future we intend to investigate alternative ways to achieve ground-state domination, e.g. simultaneous multi-state fits directly to the two- and three point functions, as well as optimizing the choice of the values of t_{sep} used in the analysis. Besides, the number of two-point function measurements on the affected ensembles may be further increased to compensate for this effect.

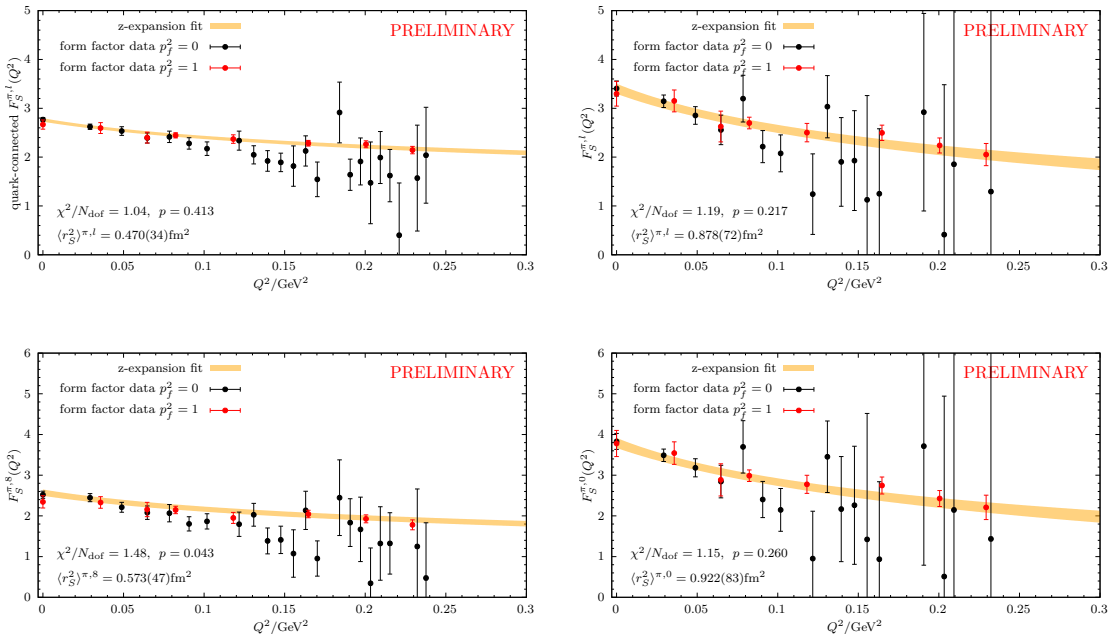

Figure 4: Unrenormalized form factor data from summation method (see text) and first order z-expansion fits on the E250 ensemble at physical light quark mass. Results are shown for the quark-connected and full light quark contribution (upper two panels), as well as the octet and singlet combinations (lower two panels). Only data for $\mathbf{p}_i^2 < 4(2\pi/l)^2$ are shown in the plots, as the signal quality rapidly deteriorates for increasing source momenta.

4. Scalar radius

Previous lattice studies had only access to very few momenta [5–7], hence they essentially used the slope between the form factor at $Q^2 = 0$ and the first one or two non-vanishing momenta to estimate the corresponding radii. The situation is quite different in the present study, as our setup allows us to compute the pion scalar form factor for a large number of different momenta with unprecedented momentum resolution on the ensembles with largest physical volume, as can be seen in Fig. 4 for the E250 ensemble at physical quark mass. The three-point function measurements

with one unit of sink momentum yield very precise results for a large range of momenta, while further refining the resolution at small momentum transfer, which is particularly beneficial for the computation of radii. In order to parametrize the form factor data in model-independent way we employ the z-expansion [31]

$$F_S^{\pi,k}(Q^2) = \sum_{n=0}^{N_z} a_n z^n \,, \qquad z = \frac{\sqrt{t_{\text{cut}} + Q^2} - \sqrt{t_{\text{cut}} - t_0}}{\sqrt{t_{\text{cut}} + Q^2} + \sqrt{t_{\text{cut}} - t_0}} \tag{9}$$

where we have $t_{\text{cut}} = 4M_\pi^2$ and use the "optimal" choice for $t_0 = t_{\text{cut}}(1 - \sqrt{1 + Q^2_{\text{max}}/t_{\text{cut}}})$. At the present level of statistical precision we find that $N_Z = 1$ yields a good description of the form factor data up to $Q^2 \leq 0.3\,\text{GeV}^2$. The scalar radii $\langle r_S^2\rangle_\pi^k$ are obtained from the a_1 coefficient in Eq. (9). Examples for the corresponding fits on our most chiral ensemble are included in Fig. 9 together with the results for the radii. The expected hierarchy of radii, i.e. $\langle r_S^2\rangle_\pi^8 < \langle r_S^2\rangle_\pi^l < \langle r_S^2\rangle_\pi^0$ is reproduced by our lattice data. There is no clear indication of lattice artifacts or finite volume effects in the data. However, obtaining final physical results for radii and $\bar{l}_4$ with fully controlled systematics will require a more detailed analysis of excited states and the Q^2-dependence of the form factor data, as well as further increasing statistics on several ensembles.

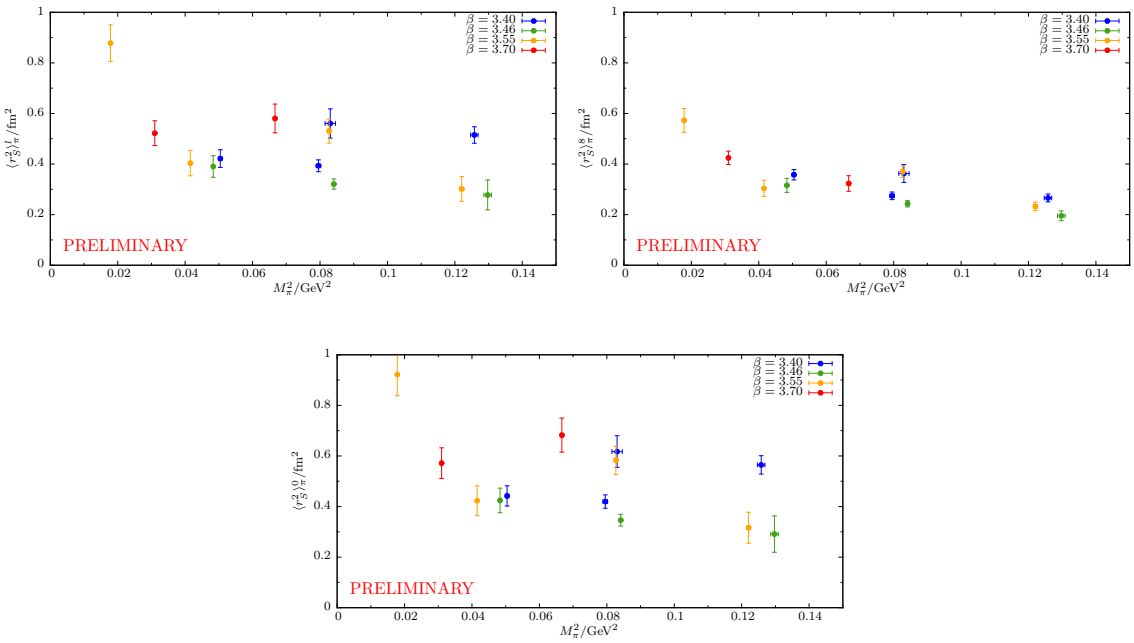

Figure 5: Results for $\langle r_S^2\rangle_\pi^l$, $\langle r_S^2\rangle_\pi^8$ and $\langle r_S^2\rangle_\pi^0$ in physical units as a function of M_π^2.

Fig. 5 shows the chiral behavior of the lattice data for $\langle r_S^2\rangle_\pi^l$, $\langle r_S^2\rangle_\pi^8$ and $\langle r_S^2\rangle_\pi^0$. The data for $\langle r_S^2\rangle_\pi^l$ are compatible with the expected logarithmic behavior for in Eq. (4). However, a few ensembles at heavier pion mass deviate from the expected curve for $\langle r_S^2\rangle_\pi^l$ and $\langle r_S^2\rangle_\pi^0$, which is caused by still insufficient effective statistics for the (2+1)-point functions at larger values of t_{sep} on these ensembles, as discussed in section 3. For the octet combination the effect is much less significant.

5. Outlook

In this proceedings contribution we have presented the status of our ongoing lattice study of the pion scalar form factor on a set of currently 13 CLS gauge ensembles. While the data production is not yet complete, and the physical extrapolation including a full error budget is still work in progress, we find that results on individual ensembles are already very competitive in terms of statistical errors when compared to previous lattice calculations. Furthermore, we achieve an unprecedented momentum resolution on boxes with large physical volumes near the physical point, which should in principle allow us to achieve a much more comprehensive assessment of systematic effects in the computation of radii.

In the future, we intend to double the number measurements for two- and three-point functions on our three most chiral ensembles (i.e. E250, E300 and D200) for which measurements are currently only available on every second gauge configuration. In addition, the number of two-point function measurements for the computation of quark-disconnected (2+1)-point functions may be further increased on selected ensembles. This concerns particularly ensembles with open boundary conditions and smaller values of T, for which statistics for these contributions is currently quite limited at larger values of t_{sep}. Moreover, we plan to extend our study to CLS ensembles on a different chiral trajectory with $m_s = \text{phys}$ to gain even better control over quark mass dependence for $\langle r_S^2 \rangle_\pi^8$ and $\langle r_S^2 \rangle_\pi^0$ when performing physical extrapolations.

Acknowledgments

This resaerch is supported by the Deutsche Forschungsgemeinschaft (DFG, German Research Foundation) through project HI 2048/1-3 (project No. 399400745). The authors gratefully acknowledge the Gauss Centre for Supercomputing e.V. (www.gauss-centre.eu) for funding this project by providing computing time on the GCS Supercomputer SuperMUC-NG at Leibniz Supercomputing Centre and on the GCS Supercomputers JUQUEEN[32] and JUWELS[33] at Jülich Supercomputing Centre (JSC). Additional calculations have been performed on the HPC clusters Clover at the Helmholtz-Institut Mainz and Mogon II and HIMster-2 at Johannes-Gutenberg Universität Mainz. We thank our colleagues in the CLS initiative for sharing gauge ensembles.

References

[1] J.F. Donoghue, J. Gasser and H. Leutwyler, *The Decay of a Light Higgs Boson*, *Nucl. Phys. B* **343** (1990) 341.

[2] J. Gasser and U.-G. Meißner, *Chiral expansion of pion form factors beyond one loop*, *Nucl. Phys. B* **357** (1991) 90.

[3] G. Colangelo, J. Gasser and H. Leutwyler, *$\pi\pi$ scattering*, *Nucl. Phys. B* **603** (2001) 125 [hep-ph/0103088].

[4] J. Gasser and H. Leutwyler, *Low-Energy Theorems as Precision Tests of QCD*, *Phys. Lett. B* **125** (1983) 325.

[5] V. Gülpers, G. von Hippel and H. Wittig, *Scalar pion form factor in two-flavor lattice QCD*, *Phys. Rev. D* **89** (2014) 094503 [1309.2104].

[6] V. Gülpers, G. von Hippel and H. Wittig, *The scalar radius of the pion from Lattice QCD in the continuum limit*, *Eur. Phys. J. A* **51** (2015) 158 [1507.01749].

[7] J. Koponen, F. Bursa, C.T.H. Davies, R.J. Dowdall and G.P. Lepage, *Size of the pion from full lattice QCD with physical u , d , s and c quarks*, *Phys. Rev. D* **93** (2016) 054503 [1511.07382].

[8] B. Sheikholeslami and R. Wohlert, *Improved Continuum Limit Lattice Action for QCD with Wilson Fermions*, *Nucl. Phys. B* **259** (1985) 572.

[9] Lüscher, M. and Weisz, P., *On-shell improved lattice gauge theories*, *Commun. Math. Phys.* **98** (1985) 433.

[10] M. Bruno et al., *Simulation of QCD with $N_f = 2 + 1$ flavors of non-perturbatively improved Wilson fermions*, *JHEP* **02** (2015) 043 [1411.3982].

[11] Lüscher, Martin and Schaefer, Stefan, *Lattice QCD with open boundary conditions and twisted-mass reweighting*, *Comput. Phys. Commun.* **184** (2013) 519 [1206.2809].

[12] M.A. Clark and A.D. Kennedy, *Accelerating dynamical fermion computations using the rational hybrid Monte Carlo (RHMC) algorithm with multiple pseudofermion fields*, *Phys. Rev. Lett.* **98** (2007) 051601 [hep-lat/0608015].

[13] S. Kuberski, *Low-mode deflation for twisted-mass and RHMC reweighting in lattice QCD*, 2306.02385.

[14] D. Mohler and S. Schaefer, *Remarks on strange-quark simulations with Wilson fermions*, *Phys. Rev. D* **102** (2020) 074506 [2003.13359].

[15] M. Bruno, T. Korzec and S. Schaefer, *Setting the scale for the CLS 2 + 1 flavor ensembles*, *Phys. Rev. D* **95** (2017) 074504 [1608.08900].

[16] M. Lüscher, *Properties and uses of the Wilson flow in lattice QCD*, *JHEP* **08** (2010) 071 [1006.4518].

[17] Flavour Lattice Averaging Group (FLAG) collaboration, *FLAG Review 2021*, *Eur. Phys. J. C* **82** (2022) 869 [2111.09849].

[18] ETM collaboration, *The eta-prime meson from lattice QCD*, *Eur. Phys. J. C* **58** (2008) 261 [0804.3871].

[19] L. Giusti, T. Harris, A. Nada and S. Schaefer, *Frequency-splitting estimators of single-propagator traces*, *Eur. Phys. J. C* **79** (2019) 586 [1903.10447].

[20] A. Stathopoulos, J. Laeuchli and K. Orginos, *Hierarchical Probing for Estimating the Trace of the Matrix Inverse on Toroidal Lattices*, *SIAM J. Sci. Comput.* **35** (2013) S299 [1302.4018].

[21] M. Cè, A. Gérardin, G. von Hippel, H.B. Meyer, K. Miura, K. Ottnad et al., *The hadronic running of the electromagnetic coupling and the electroweak mixing angle from lattice QCD*, *JHEP* **08** (2022) 220 [2203.08676].

[22] Lüscher, Martin, *Lattice QCD and the Schwarz alternating procedure*, *JHEP* **05** (2003) 052 [hep-lat/0304007].

[23] G. von Hippel, T.D. Rae, E. Shintani and H. Wittig, *Nucleon matrix elements from lattice QCD with all-mode-averaging and a domain-decomposed solver: an exploratory study*, *Nucl. Phys. B* **914** (2017) 138 [1605.00564].

[24] A. Agadjanov, D. Djukanovic, G. von Hippel, H.B. Meyer, K. Ottnad and H. Wittig, *The nucleon sigma terms with $N_f = 2+1$ O(a)-improved Wilson fermions*, 2303.08741.

[25] D. Djukanovic, G. von Hippel, H.B. Meyer, K. Ottnad, M. Salg and H. Wittig, *Electromagnetic form factors of the nucleon from $N_f = 2+1$ lattice QCD*, 2309.06590.

[26] D. Djukanovic, G. von Hippel, H.B. Meyer, K. Ottnad, M. Salg and H. Wittig, *Precision calculation of the electromagnetic radii of the proton and neutron from lattice QCD*, 2309.07491.

[27] Jüttner, Andreas, *Revisiting the pion's scalar form factor in chiral perturbation theory*, *JHEP* **01** (2012) 007 [1110.4859].

[28] L. Maiani, G. Martinelli, M.L. Paciello and B. Taglienti, *Scalar Densities and Baryon Mass Differences in Lattice QCD With Wilson Fermions*, *Nucl. Phys. B* **293** (1987) 420.

[29] S.J. Dong, K.F. Liu and A.G. Williams, *Lattice calculation of the strangeness magnetic moment of the nucleon*, *Phys. Rev. D* **58** (1998) 074504 [hep-ph/9712483].

[30] Capitani, S. and Della Morte, M. and von Hippel, G. and Jäger, B. and Jüttner, A. and Knippschild, B. and Meyer, H. B. and Wittig, H., *The nucleon axial charge from lattice QCD with controlled errors*, *Phys. Rev. D* **86** (2012) 074502 [1205.0180].

[31] G. Lee, J.R. Arrington and R.J. Hill, *Extraction of the proton radius from electron-proton scattering data*, *Phys. Rev. D* **92** (2015) 013013 [1505.01489].

[32] Jülich Supercomputing Centre, *JUQUEEN: IBM Blue Gene/Q Supercomputer System at the Jülich Supercomputing Centre*, *Journal of large-scale research facilities* **1** (2015) .

[33] Jülich Supercomputing Centre, *JUWELS Cluster and Booster: Exascale Pathfinder with Modular Supercomputing Architecture at Juelich Supercomputing Centre*, *Journal of large-scale research facilities* **7** (2021) .